Calibration of an In Situ Membrane Inlet Mass Spectrometer for Measurements of Dissolved Gases and Volatile Organics in Seawater

RYAN J. BELL,*,†,‡,§ R. TIMOTHY SHORT,‡,§ FRISO H. W. VAN AMEROM,‡,§ AND ROBERT H. BYRNE†

College of Marine Science, University of South Florida, 140 7, Avenue South, St Petersburg, Florida, 33701, Center for Ocean Technology, College of Marine Science, University of South Florida, 140 7, Avenue South, St Petersburg, Florida, 33701, and SRI International, 140 7, Avenue South COT 100, St Petersburg, Florida, 33701

Received April 17, 2007. Revised manuscript received September 07, 2007. Accepted September 09, 2007.

Use of membrane inlet mass spectrometers (MIMS) for quantitative measurements of dissolved gases and volatile organics over a wide range of ocean depths requires characterization of the influence of hydrostatic pressure on the permeability of MIMS inlet systems. To simulate measurement conditions in the field, a laboratory apparatus was constructed for control of sample flow rate, temperature, pressure, and the concentrations of a variety of dissolved gases and volatile organic compounds. MIMS data generated with this apparatus demonstrated that the permeability of polydimethylsiloxane (PDMS) membranes is strongly dependent on hydrostatic pressure. For the range of pressures encountered between the surface and 2000 m ocean depths, the pressure dependent behavior of PDMS membranes could not be satisfactorily described using previously published theoretical models of membrane behavior. The observed influence of hydrostatic pressure on signal intensity could, nonetheless, be quantitatively modeled using a relatively simple semiempirical relationship between permeability and hydrostatic pressure. The semiempirical MIMS calibration developed in this study was applied to in situ underwater mass spectrometer (UMS) data to generate high-resolution, vertical profiles of dissolved gases in the Gulf of Mexico. These measurements constitute the first quantitative observations of dissolved gas profiles in the oceans obtained by in situ membrane inlet mass spectrometry. Alternative techniques used to produce dissolved gas profiles were in good accord with UMS measurements.

Introduction

Since the late 1990s, underwater mass spectrometer (UMS) systems have been under development for direct measurements in freshwater and seawater (*1–3*). Many field portable mass spectrometers, including submersible systems, depend on the use of membrane inlets (*4–12*). Membrane inlets are advantageous as a means of reducing sample preparation requirements and decreasing gas loads on vacuum pumps. In addition, membrane inlets are rugged and allow many simple gases and volatile organic compounds (VOCs) to be monitored simultaneously (*13*).

Membrane inlet mass spectrometry (MIMS) has been used for chemical measurements since 1963 (*14*). However, many of the complexities of membrane inlet systems are still under investigation (*15–17*), and theoretical treatments of gas permeation in polymers have met with varying degrees of success (*18, 19*). Although Fick's Law describes a simple linear relationship between analyte flux and partial pressure or fugacity gradient, permeation characteristics can change when a polymer membrane undergoes compression, swelling, competitive sorption, or changes in geometry (*20*). Some of these potential complexities are not relevant to environmental measurements. For example, significant swelling and competitive sorption are not expected with aqueous samples (*21*), and properly supported membranes greatly reduce the potential significance of changes in system geometry under pressure. For aqueous samples, the principal expected influences on the behavior of membrane inlet systems are temperature, pressure, and hydrodynamics at the MIMS membrane/solution interface.

Calibration of membrane permeability as a function of temperature, pressure, and system hydrodynamics is likely to be a formidable task. In view of this expectation, it has proven advantageous to perform in situ MIMS measurements at constant temperature and flow conditions (*22*). The MIMS systems described in this work provide continuous sample-flow at constant temperature, whereupon variable hydrostatic pressure is the predominant uncontrolled influence on the membrane inlet system. Although control of hydrostatic pressure in MIMS systems is inherently feasible, such a capability is likely to substantially reduce sample throughput and add undesirable complexity to MIMS measurements. As such, to extend the capabilities of MIMS systems to observe important phenomena in the deep-sea (e.g., hydrothermal venting and benthic fluxes, including those emanating from methane hydrates), the performance of MIMS inlet systems must be characterized over a wide range of pressure.

Herein we report the effect of hydrostatic pressure on the permeability of a polydimethylsiloxane (PDMS) membrane to dissolved gases and VOCs. Physical mechanisms for hydrostatically induced variations in membrane permeability are discussed, and a semiempirical equation is developed to describe the dependence of membrane permeability on hydrostatic pressure. Our characterization of PDMS membrane behavior is used to quantitatively interpret in situ MIMS observations of dissolved gases in the Gulf of Mexico. The performance of the MIMS system is then evaluated through comparisons with measurements obtained using conventional oceanographic methods.

Theory

Steady State Permeation. The permeability (P_G) of gas G through a membrane can be described in terms of a solution-diffusion mechanism (*22*):

$$P_G = D_G K_G \tag{1}$$

where D_G is the diffusion coefficient of gas G in the membrane, and K_G is a gas partition coefficient defined as the quotient of the dissolved gas concentrations on the membrane side and the solution side of the membrane-water interface. Fick's First Law defines the gas flux (F_G) in steady state at location (x) in the membrane:

* Corresponding author e-mail: rbell@marine.usf.edu.
† University of South Florida.
‡ Center for Ocean Technology.
§ SRI International.

10.1021/es070905d CCC: $37.00
Published on Web 10/30/2007

$$F_G(x) = -P_G A\left(\frac{dC_G(x)}{dx}\right) = -D_G K_G A\left(\frac{dC_G(x)}{dx}\right) \quad (2)$$

where A is the membrane area, and $dC_G(x)/dx$ is the gas concentration gradient at x. Mass spectrometer ion current intensity is proportional to gas flux through the membrane and, for our case, can be related to sample dissolved gas concentrations via the solution to Fick's First Law for a cylindrical flow-over membrane:

$$F_G(r_i) = \frac{2\pi L D_G K_G (C_{G,2} - C_{G,1})}{\ln(r_o/r_i)} \quad (3)$$

where L is the membrane length, and ($C_{G,2}$ – $C_{G,1}$) is the difference in gas concentrations between the cylindrical membrane's outer (r_0) and inner radius (r_i). In the case that a vacuum is maintained within the membrane capillary, $C_{G,1}$is negligible compared to $C_{G,2}$.

Laminar flow at the surface of the membrane intensifies analyte depletion at the membrane surface and reduces the steady-state analyte flux (*23, 24*). Analyte depletion in the boundary layer can be partially mitigated by a high sample flow rate through restrictive geometries around the membrane. As the depletions are dependent upon sample velocity, a constant flow rate is required to obtain quantitative results.

Nonsteady-State Permeation. Characterization of nonsteady-state membrane permeation can be gained through analysis of step function dynamics. For cylindrical membrane r_o/r_i values less than about four, the theoretical solution for a stepwise increase in sample concentration is closely approximated by that of a sheet membrane (*25, 26*):

$$F_{G,t} = F_{G,ss}\left[1 + 2\sum_{n=1}^{\infty}(-1)^n \exp\left\{\frac{-n^2\pi^2 D_G t}{l^2}\right\}\right] \quad (4)$$

where l is membrane thickness, $F_{G,t}$ is gas flux at time, t, and $F_{G,ss}$ is gas flux at steady-state. Diffusion coefficients can be determined by fitting eq 4 to a concentration step function. Accurate descriptions are obtained using only a few terms in the summation.

Molar Volume Correction Factors. Pressure influences the activities of permeants in both the solution and the membrane. Changes in partition coefficients with pressure can be described in terms of the difference between the molar volumes of a given permeant in different solution phases (*27*). As such, partition coefficient variations with pressure are described as follows (*28*):

$$\frac{K_G^p}{K_G^o} = \exp[-(\Delta V_{G,m})(p - p^o)/RT] \quad (5)$$

where K_G^p is a partition coefficient at pressure p, K_G^o is a partition coefficient at standard pressure, p^o (0.101 MPa), $\Delta V_{G,m}$ is the difference between a gas partial molar volume in the membrane and the liquid phase, R is the ideal gas constant (8.31 cm^3 MPa/mol K), and T is Kelvin temperature.

Experimental Section

Laboratory Experiments. The membrane inlet assembly used in this study was developed for underwater mass spectrometry at depths to at least 2000 m, where hydrostatic pressure is approximately 20 MPa. Although this was the maximum pressure used for the tests performed here, we have observed that the membrane can support pressures of at least 40 MPa.

The membrane inlet assembly (Figure S1, Supporting Information) consisted of a hollow fiber PDMS membrane (0.064 cm i.d., 0.119 cm o.d.) (model 60–011–03; Helixmark, Carpinteria, CA) mounted in a stretched state on a porous sintered Hastelloy C rod (0.14 cm o.d. 0.75 cm length, 2 μm pore size). The supported membrane was capped on one end with a 2 mm length of polyetheretherketone (PEEK) rod (0.14 cm o.d.) and epoxy, while the other end was connected, using epoxy and a Swagelok fitting, to the vacuum chamber via a 10 cm length of stainless steel tubing (0.127 cm i.d., 0.159 cm o.d.). The membrane assembly was inserted into a stainless steel heater block (0.25 cm i.d., 3 cm o.d.) that also housed a thermocouple and heater cartridges for controlling sample and membrane temperature (+/− 0.1 °C of the set point). During variable flow experiments, a secondary heater was used to preheat samples to the set point before entry into the membrane assembly. This significantly reduced temperature fluctuations at the membrane.

The membrane inlet assembly was fitted to a Transpector 2.0 quadrupole residual gas analyzer (Inficon, Syracuse, New York) installed in a custom vacuum housing that was regulated at 100 °C. The chamber was evacuated using a turbo-molecular pump (model V70LP; Varian, Palo Alto, CA) backed by a dry diaphragm roughing pump (KNF Neuberger, Inc., Trenton, NJ). Open source electron impact ionization was performed with a thoriated tungsten filament. An electron multiplier was used for detection of ions. Samples were passed through the membrane inlet assembly at 8 mL/min using a high performance liquid chromatography (HPLC) pump (Shimadzu, Kyoto, Japan). Hydrostatic pressure at the membrane was monitored with a digital pressure gauge (Cecomp Electronics, Libertyville, IL) fitted to the sample outlet. Pressure was controlled manually using a backpressure regulator (Swagelok, Solon, OH). A schematic of the experimental setup is shown in Figure S2, Supporting Information. A pulse dampener (Restek, Bellefonte, PA) reduced pressure pulses to less than 1% of the ambient pressure. Sample flow rate was periodically measured manually to ensure that flow rates were consistent with flows defined by the HPLC pump. The maximum sample pressure was limited by the HPLC pump to 20 MPa. A stream selection valve (VICI Valco Instruments, Houston, TX) was used to control the sample introduction, and provided user-defined proportional mixing of samples to obtain calibration curves.

The primary calibration solution, containing simple dissolved gases, was prepared by sparging (>1 h) phosphate-buffered deionized water (pH 3.7, T = 25 °C) with a calibrated gas mixture (Airgas, Radnor, PA) containing 21% oxygen, 0.9% argon, 0.1% carbon dioxide, 0.1% methane, and nitrogen as the balance gas. The low pH of the phosphate-buffered solution reduced the sum concentration of HCO_3^- plus CO_3^{2-} to less than 0.3% of the total dissolved CO_2 concentration. Dissolved gas concentrations were determined using MATLAB (Version R2006a; Mathworks, Natwick, MA) scripts developed from a variety of sources (*29–33*). A second solution, deionized water at a vigorous boil (>1 h), served as a blank. A constant temperature bath (25 °C) cooled the water inline, upstream of the stream selector valve.

A third solution, containing dissolved VOCs, was prepared by addition of small quantities of dimethyl sulfide, benzene, chloroform, and toluene to 10 mL of methanol. An aliquot of the methanol solution (1.5 mL) was then added to 1 L of deionized water in a septum-sealed flask. Subsequently, sodium sulfide nonahydrate (0.2 g) and 1,4-dioxane (0.56 mL) were directly added to the 1 L solution, and monobasic potassium phosphate was used to buffer the pH to 5.3. All chemicals were obtained from Sigma-Aldrich, St. Louis, MO. Concentrations were chosen to create signal intensities that, at minimum, were an order of magnitude above the baseline values for each ion. The requisite concentrations for VOC analyses were determined by incremental additions of each VOC to an experimental solution. It was noted that, upon addition of each VOC, the ion currents for other VOCs did not change. This indicates that the m/z values chosen for quantitation of each analyte (Table 1) were free of interfer-

TABLE 1. Ions and Permeant Concentration Used for Analysis of Permeability

analyte	mass/charge	concentration (μmol/kg)
methane	15	1.4
water	17	55.6×10^6
nitrogen	28	473
methanol	30	37×10^3
oxygen	32	251
hydrogen sulfide	34	1.2×10^3
argon	40	11.8
carbon dioxide	44	34.1
dimethyl sulfide	62	100
benzene	78	9.9
chloroform	83	10
1,4-dioxane	88	6.6×10^3
toluene	91	0.99

ences, and that there was no detectable swelling of the membrane as a result of VOC sorption.

Relative changes in signal intensity were assumed to be proportional to relative changes in membrane permeability. With the exception of water, all signals were baseline subtracted. The baseline of water is known to be small relative to the signal intensity attributed to membrane permeation. Baseline values were determined by two independent methods that were in complete agreement: (1) sampling water that was being degassed by vigorous boiling; and (2) reducing of sample flow rate to zero, whereupon the aqueous sample in contact with the membrane became completely degassed. In the latter case, degassing was exponential, with 90% degassing occurring in about 1.5 min (see Figure S3, Supporting Information). The latter method is particularly convenient as it also provides a simple and effective method for the determination of baseline values in the field. Furthermore, subsequent to sample degassing, diffusion coefficients can be determined by returning the pump to its set flow rate, whereupon a step-change in concentration occurs at the membrane surface. This procedure avoids the step function dispersion that would result during propagation of a concentration interface through a length of small diameter tubing. As mass spectrometer response times are much faster than membrane response times, the observed signal step function was used to determine diffusion coefficients via eq 4 and the nonlinear fitting algorithms provided by MATLAB.

Boundary layer conditions have a strong influence on measurements of permeability and diffusion (*34*). As such, it is meaningful to report these parameters only in a relative sense, normalized to ambient atmospheric pressure. Furthermore, changes in membrane permeability due to changing hydrostatic pressure result in varying degrees of boundary layer depletion, making changes in signal intensity a summation of two influences. To address this point, experiments were performed using a range of flow rates. For the membrane inlet configuration used in the present study, variations in boundary layer depletion that resulted from changes in membrane permeability were negligible at flow rates above ~6 mL/min. Thus, changes in signal intensity with hydrostatic pressure were effectively only a function of changing membrane permeability. This is demonstrated in Figure 1 by the ratio of signal intensity at ambient pressure to signal intensity at 10 MPa, which becomes independent of flow rate at elevated flow rates.

Field Experiments. UMS field measurements were obtained using previously described instrumentation (*10*), with the following modifications: the membrane assembly was replaced with the high pressure assembly described above;

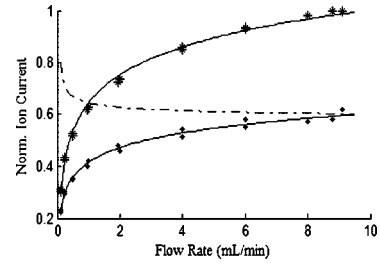

FIGURE 1. Ion current for *m/z* 28 (nitrogen) at various flow rates normalized to flow at 9 mL/min. Data were collected at ambient pressures (*) and 10 MPa (♦). The dashed line represents the ratio of data at 10 MPa to ambient pressure. A decrease in membrane permeability results in a decrease in the boundary layer thickness. Thus, the ratio increases at low flow rates. At higher flow rates, the boundary layer is small and the decease in boundary layer thickness will be insignificant compared to the change in membrane permeability. Thus, changes in ion current are a result of changes in membrane permeability.

the sample pump was replaced with a custom-made system capable of generating 10 mL/min flow rates at 42 MPa, with a power requirement near 1 W; the tungsten filament was replaced with an yttria-coated iridium filament. The Ir/Y_2O_3 filament has a lower work function than tungsten and, being inert relative to tungsten, provides longer lifetimes at elevated water and oxygen partial pressures (*35*). This reduces gas-filament reactions that have been shown to create high baselines (*14, 16*) and other problems (*36*).

Field data were collected on the West Florida Shelf in the Gulf of Mexico (27° 17.8′ N, 85° 07.9′ W) on August eighth and ninth, 2006 using the Florida Institute of Oceanography's R/V Suncoaster. The UMS was mounted on an aluminum Rosette frame (General Oceanics Inc., Miami, FL) with a custom-made battery pack, and a SBE 25 Sealogger conductivity, temperature and depth sensor (CTD) (Sea-Bird Electronics, Inc., Bellevue, WA) (Figure S4, Supporting Information). The CTD also accommodated a dissolved oxygen sensor (SBE 23). The package was deployed using a standard University National Oceanographic Laboratory System (UNOLS) oceanographic cable and winch. The battery stack consisted of 80 1.2 V "C" sized nickel metal hydride batteries. The batteries were wired to produce 24 V, and allowed continuous UMS operation for more than 8 h.

An Ethernet extender (Patton Electronics, Gaithersburg, MD) established high bandwidth real-time communications through the UNOLS cable. Although communication through the tether was intermittent due to a faulty winch slip ring, all data were recorded autonomously using the UMS embedded computer and Labview software (National Instruments, Austin, TX) whereupon data collection was not affected. The UMS computer also recorded depth, temperature, salinity, and dissolved oxygen from the CTD. Temperature and salinity data were used for calculation of seawater gas saturation states (*37*) relative to equilibrium with the atmosphere.

UMS deployment parameters were as follows: selected ion scan mode; 256 ms dwell time for *m/z* 14, 28, 32, 34, 40, 44, 62; 64 ms dwell time for *m/z* 2, 12, 15, 16, 17, 18, 20, 29, 30, 36, 45, 47, 67, 73, 78, 91, yielding a 3.5 s scan time per cycle; 1000 V electron multiplier; 40 eV electron energy; 200 mA electron current; 4 mL/min sample flow rate; and 35 °C membrane temperature. Prior to deployment, a three-point instrumental calibration was performed for methane, nitrogen, oxygen, argon, and carbon dioxide. Intercept (zero) concentrations were created at zero sample flow whereby surface seawater made stationary in contact with the membrane was completely degassed. Two additional calibration solutions were generated by sparging surface sea-

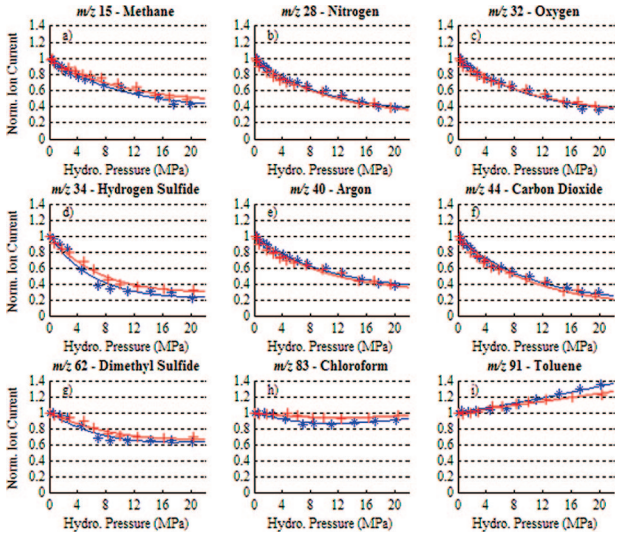

FIGURE 2. Ion current dependency on hydrostatic pressure for selected permeants at 35 °C. Blue (•) data were obtained as hydrostatic pressure was increased, and red (+) data as pressure was decreased. Data were normalized to the ion current at 0.1 MPa (ambient), and fits were obtained using eq 7.

water ($S = 36.5$, $T = 25.5$ °C) for more than 30 min with calibrated gas standards(Airgas, Radnor, PA).

Three UMS casts were performed over two days. These casts, to a depth of 500 m, were about 20 m short of the seafloor. During the first cast, the UMS sampled the water column on both the downcast and the upcast. On the subsequent cast, nine hours later, the UMS sampled a 1 L Tedlar bag (SKC Inc., Eighty Four, PA) that contained surface seawater equilibrated with a standard gas mixture. A third cast was performed the following day without the UMS. This cast was performed to examine the temperature and salinity profile of the water column. These data were absent from the first two casts due to a faulty CTD power supply. Table S1, Supporting Information outlines the sequence of events for each cast.

Results and Discussion

Laboratory Membrane Characterization. MIMS ion currents were linearly dependent on concentration at both ambient and elevated hydrostatic pressures. However, Figure 2 shows nonlinear results for MIMS ion currents plotted against hydrostatic pressure for a selection of dissolved gases and VOCs. In the case of simple gases, ion current decreases with increased pressure, indicating a decrease in membrane permeability. Larger and nonpolar permeants show an initial decrease in ion current, but an increase at higher pressure. The signal variations shown in Figure 2 are attributable to variations in membrane permeability that result from variations in diffusion coefficients and/or partition coefficients. Figure S5, Supporting Information shows that both components of permeability are pressure dependent.

Toward the goal of simple quantitative membrane inlet calibrations with respect to pressure, several models were applied to the permeability data embodied in Figure 2. However, the utility of each model was limited by (a) the large number of coefficients required to obtain acceptable data-fits and (b) unrealistic extrapolations that were obtained using the best-fit coefficients of each model. Consequently, the pressure dependence of membrane permeability for small permeants was assessed using the following simple, semiempirical model:

$$\frac{P^p}{P^o} = k + (1 - k)\exp(-b'p) \qquad (6)$$

where k corresponds to the fraction of an analyte's permeability that is independent of pressure, and b' is related to polymeric free volume and, therefore, membrane compressibility. For a given membrane, best-fit b' values are approximately constant for different permeants, while k values are specific to each permeant. For small polar compounds, k values are small, suggesting a strong permeation dependence on polymeric free volume. Large nonpolar compounds have k values near 1, indicating a minimal dependence on polymeric free volume, and a propensity for dissolution within the structure of the polymer.

Equation 6 does not predict the increase in ion current observed for many VOCs. For large permeants, a molar volume term can be included. This is achieved by combining the concepts developed in eqs 5 and 6 to produce the following semiempirical expression:

$$\frac{P^p}{P^o} = [k + (1 - k)\exp(-b'p)]\exp[-(\Delta V_{G,m})(p - p^o)/RT] \qquad (7)$$

Significant differences are expected in the molar volumes of large nonpolar molecules within a polar solvent (water) and the nonpolar polymer (PDMS). Positive increases in permeability with pressure indicate that the molar volumes of large nonpolar permeants in PDMS are smaller than in water. Equation 7 coefficients for 13 permeants were determined via nonlinear fits at 35 and 15 °C as pressure was increased (simulating downcast condition) and as pressure was decreased (simulating upcast conditions). The coefficients reported in Table S2, Supporting Information varied with temperature and membrane history, and were specific to individual membrane inlets. Notably, the temperature-dependent k values indicate that MIMS system pressure calibrations are greatly simplified by maintaining constant membrane temperature. Values for $\Delta V_{G,m}$ have the correct order of magnitude relative to those reported by Kamiya et al. (*38*). In addition, Table S2 shows that hysteresis in the MIMS response produces significant uncertainties in $\Delta V_{G,m}$ determinations. Hysteresis can be attributed to imperfect PDMS elasticity, and is consistent with compression characteristics reported in the product datasheet. Increased precision for $\Delta V_{G,m}$ and slightly better fits are achieved if b' is allowed to vary between analytes.

Field Data. Several UMS dissolved gas profiles obtained in the Gulf of Mexico are presented in Figure 3. VOC depth profiles were, as expected in the open ocean, below instrument detection limits. Figures 3a–c show UMS signals at m/z 17 (water), m/z 28 (nitrogen) and m/z 32 (oxygen) expressed in terms of concentrations via calibrations at one atmosphere hydrostatic pressure. Water activity is dependent on temperature and, to a lesser extent, salinity. Since the membrane temperature was 35 °C and salinity was essentially constant between the surface and 500 m, the water profile shows a decrease with depth that must be attributable to compression of the PDMS membrane. Nitrogen and oxygen profiles differ distinctly from the water profile. Nitrogen concentrations in seawater are strongly dominated by ambient seawater temperature and salinity during equilibration with the atmosphere. Since neither temperature nor nitrogen concentrations are substantially altered during water mass subduction, the nitrogen profile shown in Figure 3b increases with depth in response to decreasing in situ temperature. Oxygen concentrations are influenced strongly by both physical and biological processes. Subsequent to atmospheric equilibrium, dissolved oxygen concentrations are, like nitrogen, inversely related to both temperature and salinity. Photosynthesis at shallow depths typically produces small supersaturations with respect to atmospheric equilibrium, and net respiration at greater depths typically reduces

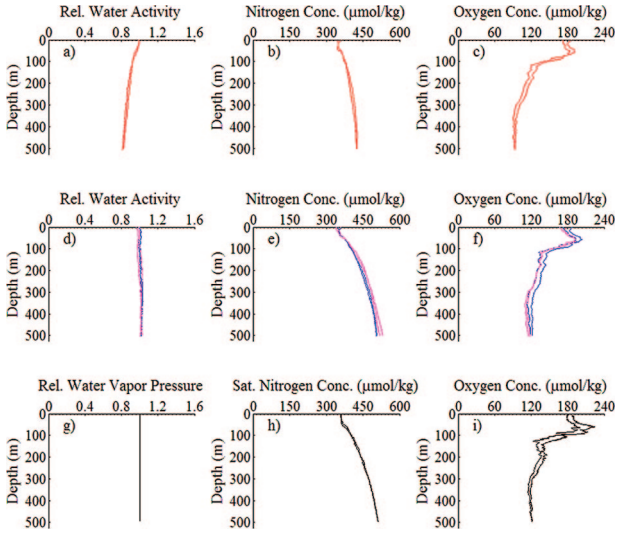

FIGURE 3. Concentration depth profiles (downcast and upcast) from the Gulf of Mexico. Figures a–c were obtained using 0.1 MPa concentration calibrations. Figures d–f show pressure corrected data; the blue lines were corrected using eq 7, and the magenta lines were corrected using data obtained with a standard solution. Figures g–i show data determined with an independently deployed CTD and oxygen sensor.

oxygen concentrations to levels much below saturation. All of these influences are seen in Figure 3c.

Although the influence of membrane compression on signal intensities is seen most clearly in Figure 3a, it is apparent that membrane compression is an important effect for all UMS observations. Two independent methods were used to account for the effects of hydrostatic pressure on instrument response. In the first case, calibration coefficients obtained via eq 6 were used to generate the activity and concentration profiles shown (blue) in Figures 3d–f. Although this method is complicated by calibration coefficients that may vary between casts, it provides an essential first order account of pressure-corrected instrument response when deployment logistics do not allow in situ calibration, as described below.

As an alternative to pressure corrections via eq 6, the pressure dependence of UMS signals were examined while the UMS sampled a standard solution during a follow-up profile to 500 m. The data from this follow-up profile were normalized to the UMS signal intensities obtained while the standard solution was sampled at the surface. High frequency noise was smoothed using a fourth degree polynomial fit. These data were then used to correct the raw in situ data obtained during the first cast. The results obtained in this analysis, which provide a first order account of the influence of membrane deformation kinetics on UMS measurements, are shown (magenta, downcast and upcast) in Figures 3d–f The juxtaposition of magenta and blue profiles shows no systematic depth-dependent differences between calibration methods. As such, it appears that hysteresis is a minor influence in the upper 500 m and can be accounted for quantitatively. Nevertheless, it should be noted that this type of procedure should become increasingly important if UMS observations were to include a wider range of depth in the water column.

Figures 3g–i show activity and concentration profiles that were determined independent of UMS observations. Water vapor pressure, calculated from salinity (*39*) and normalized to vapor pressure at the sea surface, is shown vs depth in Figure 3g. As directly observed in Figure 3d, in the absence of strong salinity gradients, variations in water activity (and hence vapor pressure) are expected to be very small. Figure 3h shows predicted nitrogen saturation concentrations (calculated from temperature and salinity) for equilibrium with the atmosphere. Good accord is observed with the UMS data shown in Figure 3e. Figure 3i shows a dissolved oxygen profile obtained with the SBE 23 dissolved oxygen sensor. The data shown in Figures 3f and i are in very good agreement, and it can be noted that, due to hysteresis effects, the dissolved oxygen sensor shows downcast/upcast differences that are generally as large or larger than those obtained by the UMS. These measurements, which constitute the first quantitative observations of dissolved gas profiles in the oceans obtained by in situ membrane inlet mass spectrometry, indicate that UMS systems are capable of providing unique quantitative assessments of fine-scale processes in the marine environment.

Acknowledgments

We gratefully acknowledge the assistance of Strawn K. Toler, Gottfried Kibelka, Peter G. Wenner, Lori R. Adornato, and the staff at the USF Center for Ocean Technology throughout the UMS development process. This work was supported by funding from the U.S. Office of Naval Research (grant no. N00014-03-1-0479). Cruise time was supported through U.S. Office of Naval Research (grant no. N00014-03-1-0612).

Supporting Information Available

Supplemental figures, tables and discussion are available in the Supporting Information. This material is available free of charge via the Internet at http://pubs.acs.org.

Literature Cited

(1) Gereit, F.; Hauptmann, P.; Matz, G.; Mellert, V.; Reuter, R. *an Rov-Based Sensor System for Maritime Pollution Control*; Ocean. Int. 98: Brighton, UK, 1998.

(2) Hemond, H.; Camilli, R. NEREUS: engineering concept for an underwater mass spectrometer. *TrAC, Trends Anal. Chem.* **2002**, *21* (8), 526–533.

(3) Short, R. T.; Fries, D. P.; Toler, S. K.; Lembke, C. E.; Byrne, R. H. Development of an underwater mass-spectrometry system for in situ chemical analysis. *Meas. Sci. Technol.* **1999**, *10* (12), 1195–1201.

(4) Janfelt, C.; Frandsen, H.; Lauritsen, F. R. Characterization of a mini membrane inlet mass spectrometer for on-site detection of contaminants in both aqueous and liquid organic samples. *Rapid Commun. Mass Spectrom.* **2006**, *20*, 1441–1446.

(5) Johnson, R. C.; Cooks, R. G.; Allen, T. M.; Cisper, M. E.; Hemberger, P. H. Membrane introduction mass spectrometry: Trends and applications. *Mass Spectrom. Rev.* **2000**, *19* (1), 1–37.

(6) Kotiaho, T. On-site environmental and in situ process analysis by mass spectrometry. *J. Mass Spectrom.* **1996**, *31* (1), 1–15.

(7) Matz, G.; Kibelka, G.; Dahl, J.; Lennemann, F. Experimental study on solvent-less sample preparation methods-Membrane extraction with a sorbent interface, thermal membrane desorption application and purge-and-trap. *J. Chromatogr., A* **1999**, *830* (2), 365–376.

(8) Tortell, P. D. Dissolved gas measurements in oceanic waters made by membrane inlet mass spectrometry. *Limnol. Oceanogr. Methods* **2005**, *3*, 24–37.

(9) Short, R. T.; Toler, S. K.; Kibelka, G. P. G.; Rueda Roa, D. T.; Bell, R. J.; Byrne, R. H. Detection and quantification of chemical plumes using a portable underwater membrane introduction mass spectrometer. *TrAC, Trends Anal. Chem.* **2006**, *25* (7), 637–646.

(10) Short, R. T.; Fries, D. P.; Kerr, M. L.; Lembke, C. E.; Toler, S. K.; Wenner, P. G.; Byrne, R. H. Underwater mass spectrometers for in situ chemical analysis of the hydrosphere. *J. Am. Soc. Mass. Spectrom.* **2001**, *12* (6), 676–682.

(11) Camilli, R.; Hemond, H. F. NEREUS/Kemonaut, a mobile autonomous underwater mass spectrometer. *TrAC, Trends Anal. Chem.* **2004**, *23* (4), 307–313.

(12) Bossuyt, A.; McMurtry, G. M. *A Deep-Sea Mass Spectrometer Instrument for Long-Term, In Situ Biogeochemical Monitoring, Fall 2004*; AGU: San Fransisco, CA. 2004.

(13) Thompson, A. J.; Creba, A. S.; Ferguson, R. M.; Krogh, E. T.; Gill, C. G. A coaxially heated membrane introduction mass spec-

trometry interface for the rapid and sensitive on-line measurement of volatile and semi-volatile organic contaminants in air and water at parts-per-trillion levels. *Rapid Commun. Mass Spectrom.* **2006**, *20* (13), 2000–2008.
(14) Hoch, G.; Kok, B. A mass spectrometer inlet system for sampling gases dissolved in liquid phases. *Arch. Biochem. Biophys.* **1963**, *101*, 160–170.
(15) Futo, I.; Degn, H. Effect of sample pressure on membrane inlet mass spectrometry. *Anal. Chim. Acta* **1994**, *294* (2), 177–184.
(16) Oersnes, H.; Bohatka, S.; Degn, H. Reaction of water at hot filament interferes with measurements of dissolved gases by membrane inlet mass spectrometry. *Rapid Commun. Mass Spectrom.* **1997**, *11* (15), 1736–1738.
(17) Hansen, K. F.; Gylling, S.; Lauritsen, F. R. Time- and concentration-dependant relative peak intensities observed in electon impact membrane inlet mass spectra. *Int. J. Mass Spectrom. Ion Process.* **1996**, *152* (2–3), 143–155.
(18) Klopffer, M. H.; Flaconneche, B. Transport properties of gases in polymers: bibliographic review. *Oil Gas Sci. Technol.* **2001**, *56* (3), 223–244.
(19) Lipnizki, F.; Trägårdh, G. Modelling of pervaporation: models to analyze and predict the mass transport in pervaporation. *Sep. Purif. Methods* **2001**, *30* (1), 49–125.
(20) Fujita, H. Diffusion in polymer-diluent systems. *Algebra Univ.* **1961**, *3* (1), 1–47.
(21) Favre, E.; Schaetzel, P.; Nguygen, Q. T.; Clement, R.; Neel, J. Sorption, diffusion and vapor permeation of various penetrants through dense poly (dimethylsiloxane) membranes: a transport analysis. *J. Membr. Sci.* **1994**, *92*, 169–184.
(22) LaPack, M. A.; Tou, J. C.; Enke, C. G. Membrane mass spectrometry for the direct trace analysis of volatile organic compounds in air and water. *Anal. Chem.* **1990**, *62* (13), 1265–1271.
(23) Sysoev, A. A. A Mathematical Model for Kinetic Study of Analyte Permeation from Both Liquid and Gas Phases through Hollow Fiber Membranes into Vacuum. *Anal. Chem.* **2000**, *72* (17), 4221–4229.
(24) Woldring, S. Biomedical application of mass spectrometry for monitoring partial pressures. A technical review. *J. Assoc. Adv. Med. Instrum.* **1970**, *4* (2), 43–56.
(25) Pasternak, R. A.; Schimscheimer, J. F.; Heller, J. A dynamic approach to diffusion and permeation measurements. *J. Polym. Sci., Part A: Polym. Phys.* **1970**, *8* (3), 467–479.
(26) Crank, J. *the Mathematics of Diffusion*, 2nd ed.; Clarendon Press: Oxford, 1975.
(27) Wijmans, H. G. The role of permeant molar volume in the solutuion-diffusion model transport equations. *J. Membr. Sci.* **2004**, *237* (1–2), 39–50.
(28) Millero, F. J. *Chemical Oceanography*: CRC Press: Boca Raton, FL,1983; Vol. 8, pp 1–88.
(29) Weiss, R. F. The solubility of nitrogen, oxygen and argon in water and seawater. *Deep-Sea Res.* **1970**, *17*, 721–735.
(30) Weiss, R. F. Carbon dioxide in water and seawater: the solubility of a non-ideal gas. *Mar. Chem.* **1974**, *2* (3), 203–215.
(31) Hamme, R. C.; Emerson, S. R. The solubility of neon, nitrogen and argon in distilled water and seawater. *Deep-Sea Res., Part I* **2004**, *51* (11), 1517–1528.
(32) Wiesenburg, D. A.; Guinasso Jr, N. L. Equilibrium solubilities of methane, carbon monoxide, and hydrogen in water and sea water. *J. Chem. Eng. Data* **1979**, *24* (4), 356–360.
(33) Garcia, H. E.; Gordon, L. I. Oxygen solubility in seawater: Better fitting equations. *Limnol. Oceanogr.* **1992**, *37* (6), 1307–1312.
(34) Krogh, E. T.; Pel, D. M. v.; Lynch, M. S.; Gill, C. G.; Durning, C. J.; Janes, D. *Measurement of Environmentally Relevant Partition and Diffusion Coefficients Using Membrane Introduction Mass Spectrometry*, 54th ASMS Conference on Mass Spectrometry, Seattle, WAq, **2006**.
(35) Harvey, F. J. High temperature oxidation of tungsten wires in water vapor-argon mixtures. *Metall. Trans.* **1974**, *5*, 1189–1192.
(36) Kana, T. M.; Weiss, D. L.; Eyre, B. E.; Rysgaard, S.; Dalsgaard, T.; Christensen, P. B. Comment on: "Comparison of isotope pairing and N_2:Ar methods for measuring sediment denitrification" by Eyre, B.D. et al. Authors' reply. *Estuaries.* **2004**, *27* (1), 173–178.
(37) Hamme, R. C.; Emerson, S. R. Mechanisms controlling the global oceanic distribution of the inert gases argon, nitrogen and neon. *Geophys. Res. Lett.* **2002**, *29* (23), 35–31.
(38) Kamiya, Y.; Naito, Y.; Terada, K.; Mizoguchi, K. Volumetric properties and interaction parameters of dissolved gases in poly (dimethylsiloxane) and polyethylene. *Macromolecules* **2000**, *33* (8), 3111–3119.
(39) Hamme, R.,Gas Solubility Matlab Functions, http://web.uvic.ca/~rhamme/download.html, Sept. 2006.

ES070905D